Journal of Power Sources 210 (2012) 172–177

Contents lists available at SciVerse ScienceDirect

Journal of Power Sources

journal homepage: www.elsevier.com/locate/jpowsour

Short communication

Electrochemical investigation of strontium doping effect on high performance $Pr_{1-x}Sr_xCoO_{3-\delta}$ ($x = 0.1$, 0.3, 0.5, and 0.7) cathode for intermediate-temperature solid oxide fuel cells

Seonhye Park[a], Sihyuk Choi[a], Jeeyoung Shin[b], Guntae Kim[a,*]

[a] Interdisciplinary School of Green Energy, Ulsan National Institute of Science and Technology (UNIST) and UNIST-KIER Advanced Center for Energy, Ulsan 689-798, Republic of Korea
[b] Department of Mechanical Engineering, Dong-Eui University, Busan 614-714, Republic of Korea

ARTICLE INFO

Article history:
Received 16 January 2012
Received in revised form 6 March 2012
Accepted 10 March 2012
Available online 21 March 2012

Keywords:
Solid oxide fuel cells
Cathode
Perovskite
Oxygen non-stoichiometry
Electrochemical performance

ABSTRACT

The $Pr_{1-x}Sr_xCoO_{3-\delta}$ perovskite-type oxides have received extensive attention as a promising cathode material due to their favorable properties for realizing high performance intermediate temperature solid oxide fuel cells (IT-SOFCs). This study focuses on the electrical properties, electrochemical performance, and redox behavior of a perovskite oxide of $Pr_{1-x}Sr_xCoO_{3-\delta}$ ($x = 0.1$, 0.3, 0.5, and 0.7). For $x = 0.1$ and 0.3, the electrical conductivities increase with increasing strontium content. In the case of $x > 0.3$, however, decreased electrical conductivity is observed with increasing x. The oxygen non-stoichiometry of $Pr_{1-x}Sr_xCoO_{3-\delta}$ using coulometric titration and its electrical conductivity in a wide range of oxygen partial pressure at 973 K are also investigated. A Ni-GDC anode-supported cell is fabricated to evaluate the electrochemical performance of the $Pr_{1-x}Sr_xCoO_{3-\delta}$ cathode material. The maximum power density at 973 K is 1.19 W cm^{-2} for $x = 0.3$, and the other samples also show high power density over 1.0 W cm^{-2}, except for at $x = 0.7$. Given its high electrical conductivity and cell performance, $Pr_{0.7}Sr_{0.3}CoO_{3-\delta}$ is a favorable cathode material candidate for IT-SOFC applications.

1. Introduction

Solid oxide fuel cells (SOFCs) offer numerous advantages for power generation, including high efficiency to generate electric energy from chemical energy, rapid reaction kinetics, an eco-friendly process, and efficient reclamation of waste heat. High operating temperature (1073–1273 K), however, leads to high cost and undesired reactions between the electrode and electrolyte, which in turn cause electrode densification and polarization. Recently, intermediate temperature solid oxide fuel cells (IT-SOFCs) operated at 773–973 K have been introduced to resolve the problem of high operating temperature of SOFCs, thereby allowing long-term stability and flexible choice in cell materials. The lowered operating temperature, however, causes relatively slow reaction kinetics for the oxygen reduction reaction (ORR) at the cathode, which results in considerable over-potential at the interface between the electrode and electrolyte. Therefore, the development of new cathode materials for lower operating temperature is considered an important avenue of research for IT-SOFC applications [1–5].

The requirements of cathode materials for IT-SOFCs are high oxide ionic and electronic conductivities, lower thermal expansion, and high catalytic activity for the ORR [6]. Mixed ionic/electronic conductors (MIECs) containing Mn, Fe, Co, and/or Ni are IT-SOFC cathode materials, offering the capability to conduct oxygen ions and electrons simultaneously, leading to enlarged triple phases boundary (TPB) sites [7–10]. In particular, various MIEC oxides containing cobalt oxides, such as $LaCoO_3$, (La, Sr)CoO_3, $BaCoO_3$, and (Ba, Sr)CoO_3, have attracted strong interest due to their high electro-catalytic activity for the ORR. Recently, Sr doped rare-earth cobalt oxides, $Ln_{1-x}Sr_xCoO_{3-\delta}$ (Ln = La, Pr, Nd, Sm, and Gd), have been extensively investigated on the basis of their good mixed conductivity and performance as IT-SOFC cathode materials [11–15]. Among them, $La_{1-x}Sr_xCoO_{3-\delta}$ shows better electrical properties and higher catalytic activity, as well as good thermal stability at various temperatures and oxygen partial pressure [16,17]. $La_{1-x}Sr_xCoO_{3-\delta}$ cathodes, however, show an increased thermal expansion coefficient (TEC) caused by the increased Ln–O bond strength and the formation of oxide ion vacancies, indicating reduction of the smaller Co^{4+} ions to larger Co^{3+} ions [18]. In order to achieve lower thermal expansion, the La lanthanide is substituted by other smaller lanthanides to decrease the ionicity of the Ln–O bond and the electro-negativity of Ln. Among the smaller lanthanides (Pr, Nd, Sm, and Gd), Pr affords a relatively lower TEC than La and higher electrical conductivity and electrochemical performance than Nd, Sm, and Gd due to its comparatively straightened Co–O–Co bond angle approaching 180° and a consequent increase in bandwidth [11,18]. Therefore, a Sr doped rare-earth

* Corresponding author. Tel.: +82 52 217 2917; fax: +82 52 217 2909.
E-mail address: gtkim@unist.ac.kr (G. Kim).

0378-7753/$ – see front matter.
doi:10.1016/j.jpowsour.2012.03.018

cobalt oxide, $Pr_{1-x}Sr_xCoO_{3-\delta}$, has been studied as a prospective cathode material for IT-SOFC applications.

This study mainly focuses on the structure, electrochemical properties, and electrical performances of $Pr_{1-x}Sr_xCoO_{3-\delta}$ (x = 0.1, 0.3, 0.5, and 0.7) using $Ce_{0.9}Gd_{0.1}O_{1.95}$ (GDC) electrolyte to eliminate inappropriate reactions between the electrolyte and cathode. For example, the reaction between $La_{1-x}Sr_xCoO_{3-\delta}$ and yttria stabilized zirconia (YSZ) electrolyte stimulates the formation of $La_2Zr_2O_7$ and $SrZrO_3$ at high temperature [19]. Additionally, oxygen non-stoichiometry and redox properties of $Pr_{1-x}Sr_xCoO_{3-\delta}$ are measured by coulometric titration (CT).

2. Experimental

$Pr_{1-x}Sr_xCoO_{3-\delta}$ oxides were synthesized by the Pechini method to fabricate samples for evaluation of the 4-probe conductivity and coulometric titration. The solution was prepared with stoichiometric amounts of $Pr(NO_3)_3{\cdot}6H_2O$ (Aldrich, 99.9%, metal basis), $Sr(NO_3)_2$ (Aldrich, 99+%), and $Co(NO_3)_2{\cdot}6H_2O$ (Aldrich, 98+%) with the addition of ethylene glycol and citric acid as heterogeneous agents in distilled water. The solution was heated until submicron powder particles were formed via a self-combustion process. These powders were precalcined at 873 K for 2 h and then ball-milled in acetone for 24 h. For the final step to achieve a single phase, the powders were pelletized at 5 MPa and then sintered at 1423 K for 4 h in air.

The glycine-nitrate process (GNP), which can produce fine particles, was used to prepare $Pr_{1-x}Sr_xCoO_{3-\delta}$ for the cathode and GDC powder for the electrodes and electrolyte. The glycine was applied to the solution at a molar ratio of 1:1.5 for metal nitrate and glycine. To measure cell performances of the $Pr_{1-x}Sr_xCoO_{3-\delta}$ cathodes, the powders and GDC were mixed at a weight ratio of 6:4 and ball-milled for 24 h. The electrode powders were blended with an organic binder (Heraeus V006) to form slurries for a cell test.

All samples were identified by X-ray powder diffraction (XRD) (Rigaku-diffractometer, Cu Ka radiation) patterns. To confirm the microstructure of the interface between the GDC electrolyte and $Pr_{1-x}Sr_xCoO_{3-\delta}$ cathodes, a field emission scanning electron microscope (SEM) (Nova SEM) was used. A thermogravimetric analysis (TGA) was carried out using a SDT-Q600 (TA instrument, USA). TGA experiments were performed from 373 K to 1073 K with a heating/cooling rate of 2 K min^{-1} in air. The electrical conductivities of the $Pr_{1-x}Sr_xCoO_{3-\delta}$ oxides with average dimensions of 1.4 mm × 2.7 mm × 5.5 mm in air were evaluated by a four-terminal DC arrangement, and a potentiostat (BioLogic) was used to measure the current and voltage at intervals of 50 K at temperature ranging from 373 K to 1023 K.

The redox properties of the $Pr_{1-x}Sr_xCoO_{3-\delta}$ oxides were measured using coulometric titration (CT) as a function of the oxygen partial pressure, $p(O_2)$. The detailed procedure has been described elsewhere [20]. The sample was placed inside an oxygen ion (O^{2-}) conducting membrane, a YSZ tube (McDanel Advanced Ceramic Technologies, Z15410630). Ag paste (SPI Supplies, 05063-AB) was painted on the inner and outer walls of the tube as electrodes. Pt wire was used as a lead wire to make electrical connections to the instruments. After purging 5% O_2–Ar gas over the sample in the tube for 12 h, $p(O_2)$ was determined from the open-circuit voltage (OCV). Oxygen could be added or removed from the tube by passing current through the same electrodes as used for the OCV sensor. The sample was allowed to equilibrate until the potential varied in a range of less than 1 mV h^{-1}. Oxygen non-stoichiometry was determined through this procedure at 973 K over a wide range of oxygen partial pressure. Electrical conductivity was simultaneously measured by a four-terminal DC arrangement with a BioLogic Potentiostat.

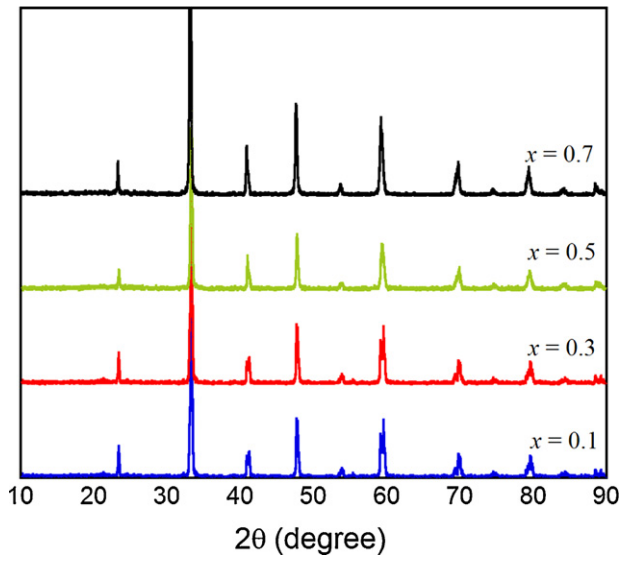

Fig. 1. X-ray diffraction patterns of $Pr_{1-x}Sr_xCoO_{3-\delta}$ (x = 0.1, 0.3, 0.5, and 0.7) sintered at 1423 K for 4 h.

For evaluation of the electrochemical performances, Ni-GDC anode-supported cells were used. The cells consist of 3 layers: Ni-GDC as an anode, GDC as an electrolyte, and a cathode. The Ni-GDC cermet anode was fabricated from a mixture of nickel oxide, GDC prepared by GNP, and starch at a weight ratio of 6:4:1.5. This mixture was ball-milled in ethanol for 24 h. The GDC powder electrolyte was pressed over the pelletized Ni-GDC cermet anode. The Ni-GDC/GDC anode-electrolyte layer was sintered at 1623 K for 5 h. For the top layer cathode, the $Pr_{1-x}Sr_xCoO_{3-\delta}$ oxide slurries were screen-printed on the GDC electrolyte. The cells, with an active electrode area of 0.36 cm^2, were finally sintered at 1173 K for 2 h under an air atmosphere. The single cells had the following properties: diameter of 0.36 cm^2, electrolyte thickness of 20–30 μm, cathode thickness of 20 μm, cathode porosity of approximately 30%, and mean pore size of 1 μm. Ag wires were attached to both the anode and cathode of a single cell using Ag paste as a current collector. An alumina tube was employed to fix the single cell using a ceramic adhesive (Aremco, Ceramabond 553). H_2 containing 3% H_2O was applied through a water bubbler with a flow rate of 20 mL min^{-1}, while air was applied as an oxidant and supplied to the cathode by ambient air flow during the single cell test. A BioLogic Potentiostat was used to measure impedance spectra and I–V curves. Impedance spectra were recorded under OCV in a frequency range of 1 mHz to 500 kHz with AC perturbation of 14 mA at 973 K. I–V polarization curves were measured between 773 K and 973 K.

3. Results and discussion

The XRD patterns of $Pr_{1-x}Sr_xCoO_{3-\delta}$ cathodes with various strontium content (x = 0.1, 0.3, 0.5, and 0.7) are shown in Fig. 1. $Pr_{1-x}Sr_xCoO_{3-\delta}$ oxides sintered at 1423 K for 4 h show appropriate peaks, indicating that the perovskite structure is formed and there are no impurity peaks. The peaks reflect an orthorhombic perovskite GdFeO-type structure (space group Pbnm) [21]. The XRD spectra of $Pr_{1-x}Sr_xCoO_{3-\delta}$–GDC powder composites calcined at 1173 K for 2 h in air are illustrated in Fig. 2. There are no obvious reactions between $Pr_{1-x}Sr_xCoO_{3-\delta}$ and GDC at 1173 K and the patterns verify that all samples obtain a stable perovskite structure. Secondary phases are observed at approximately $2\theta = 32.2^\circ$ and indexed to a tetragonal system [21].

The microstructure of the $Pr_{1-x}Sr_xCoO_{3-\delta}$ cathode is examined by SEM image in Fig. 3. The electrode microstructure is related to the

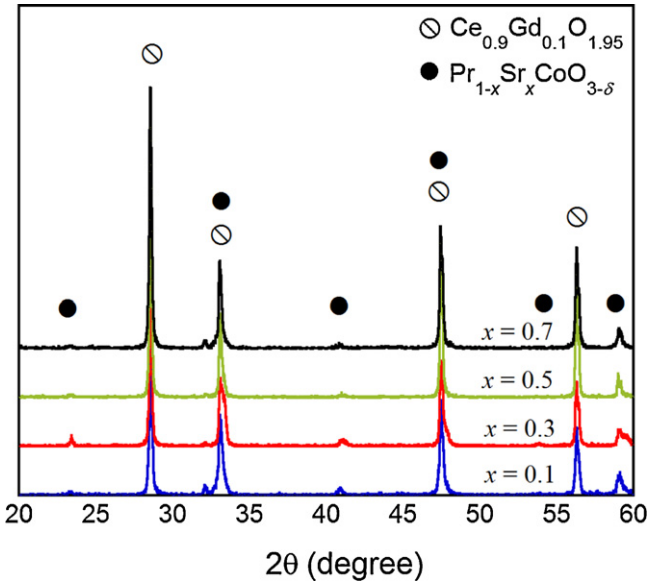

Fig. 2. X-ray diffraction patterns of $Pr_{1-x}Sr_xCoO_{3-\delta}$–GDC ($x$ = 0.1, 0.3, 0.5, and 0.7) sintered at 1173 K for 2 h.

characteristics of the surface area, electrochemically active area, volume fraction of chemical phases present, and electron transport. These properties affect the reaction kinetics, charge transport, and mass transport processes, which are correlative with the fuel cell performance [22,23]. SEM images of $Pr_{1-x}Sr_xCoO_{3-\delta}$ screen printed onto the GDC electrolyte confirm good adhesion between the cathode and the GDC electrolyte, which is expected to enhance the thermal compatibility and the long-term thermal stability of the cathode/electrolyte interface. The particle size of all samples are similar except for x = 0.7, where the particles are slightly larger than those of the other samples. Therefore, it is believed that the microstructure of $Pr_{1-x}Sr_xCoO_{3-\delta}$ does not significantly affect the electrochemical characteristics.

Thermogravimetric analysis (TGA) data of $Pr_{1-x}Sr_xCoO_{3-\delta}$ are shown in Fig. 4. The TGA data describe the tendency of oxygen nonstoichiometry (vacancy concentration) of $Pr_{1-x}Sr_xCoO_{3-\delta}$. All samples initiate a weight change at approximately 573 K. The magnitude of the weight change, indicating a loss of oxygen from the lattice in $Pr_{1-x}Sr_xCoO_{3-\delta}$, decreases in the order of x = 0.7 > 0.5 > 0.1 > 0.3. This oxygen vacancy formation can be associated with Co reduction due to the charge compensation mechanism.

The electrical conductivities of the $Pr_{1-x}Sr_xCoO_{3-\delta}$ are described by an Arrhenius plot in Fig. 5. All samples show decreased electrical conductivities with increasing temperature, indicating metallic behavior. At higher temperatures (>673 K), the electrical

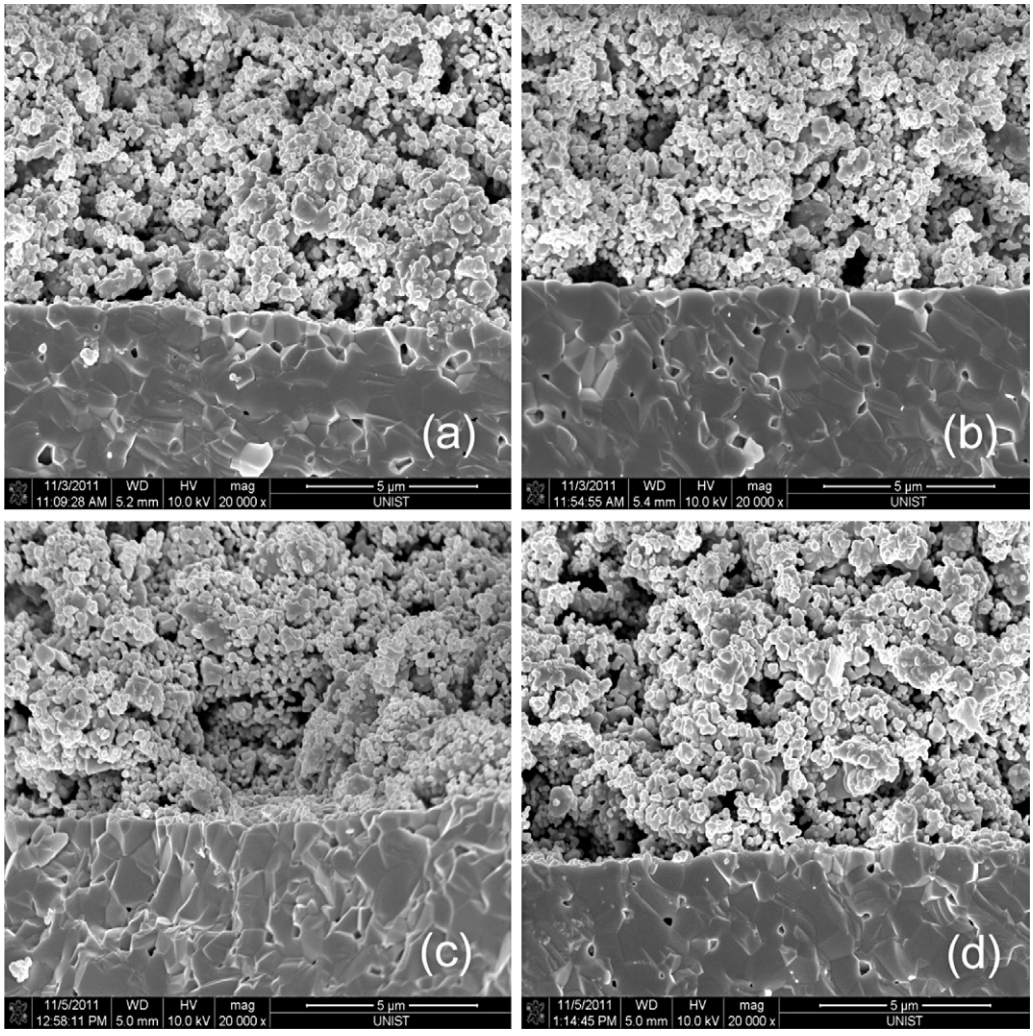

Fig. 3. SEM images showing the microstructure of a single cell ($Pr_{1-x}Sr_xCoO_{3-\delta}$–GDC/GDC/Ni-GDC): (a) x = 0.1, (b) x = 0.3, (c) x = 0.5, and (d) x = 0.7.

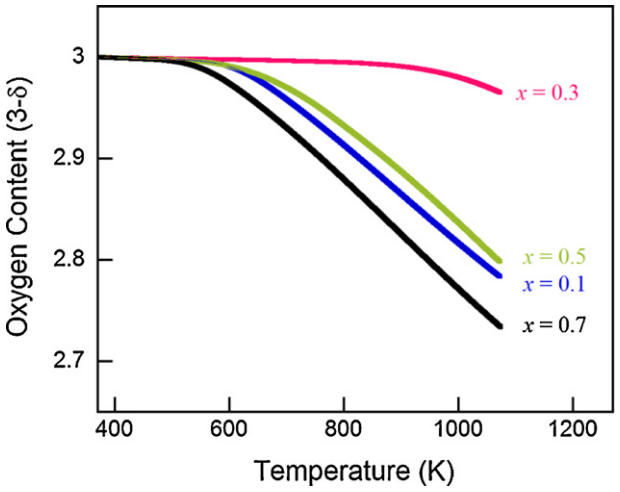

Fig. 4. Thermogravimetric data of $Pr_{1-x}Sr_xCoO_{3-\delta}$ ($x = 0.1, 0.3, 0.5$, and 0.7) showing the variation of oxygen content as a function of temperature in air.

conductivities for all samples decrease significantly with temperature; this could be due to the loss of oxygen from the lattice, as indicated by the TGA data, and a consequent decrease in the Co^{4+} charge carrier concentration. As can be seen, the electrical conductivity of the sample with $x = 0.3$ reaches a maximum with a value of 2000 S cm^{-1} at 973 K in air. Therefore, in $Pr_{1-x}Sr_xCoO_{3-\delta}$, the electrical conductivity increases with the amount of strontium doping for $x \leq 0.3$ but decreases for $x > 0.3$.

The replacement of Pr^{3+} by Sr^{2+} in $Pr_{1-x}Sr_xCoO_{3-\delta}$ destroys the electro-neutrality, which is mostly compensated by oxidation of Co^{3+} to Co^{4+} (electronic compensation) and/or the formation of oxide ion vacancies (ionic compensation) [11]. Generally, the electronic compensation mechanism is dominant at high oxygen partial pressures and low temperatures while the ionic compensation mechanism conversely dominates at low oxygen partial pressures and high temperatures. The increased conductivity with increasing Sr (Sr^{2+}) content for $x \leq 0.3$ can be explained by the fact that the formation of Co^{4+} ions prevails over the formation of oxygen vacancies to compensate the electro-neutrality. In contrast, the decreased conductivity with increasing Sr content for $x > 0.3$ indicates that the ionic compensation is dominant compared to electronic compensation. The overall electro neutrality condition can be explained by the following simplified equation:

$$\left[Sr'_{Pr}\right] = \left[Co^{\bullet}_{Co}\right] + 2\left[V^{\bullet\bullet}_{o}\right]$$

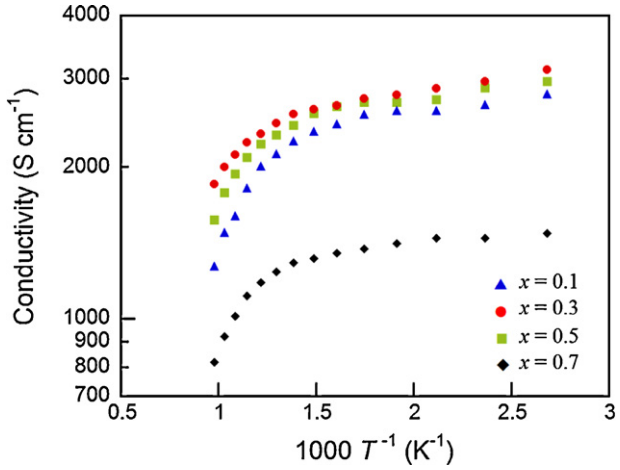

Fig. 5. Electrical conductivities of $Pr_{1-x}Sr_xCoO_{3-\delta}$ ($x = 0.1, 0.3, 0.5$, and 0.7) in air as a function of temperature.

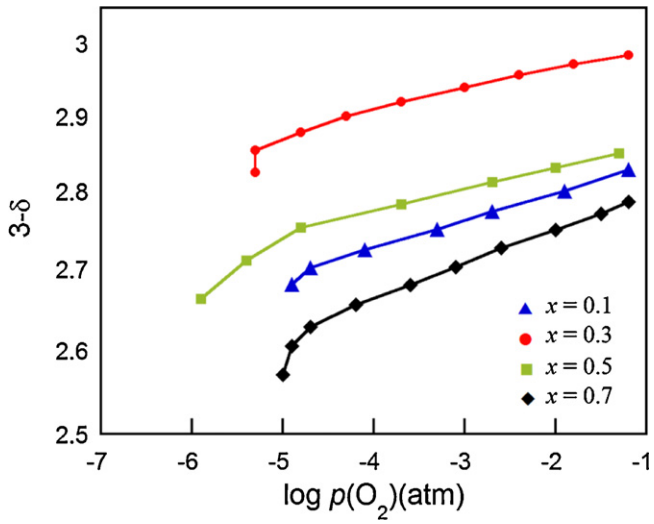

Fig. 6. Oxygen non-stoichiometry of $Pr_{1-x}Sr_xCoO_{3-\delta}$ ($x = 0.1, 0.3, 0.5$, and 0.7) at 973 K by coulometric titration.

Petrov's group [24], using iodometric titration, reported that the concentration of Co^{4+} in a $La_{1-x}Sr_xCoO_{3-\delta}$ system is increased with x, reaches a maximum at $x = 0.4$, and then decreases. In other words, the electro-neutrality is accommodated primarily by the ionic mechanism at higher doping levels ($x > 0.4$). These ionic and electronic mechanisms could be distinguished by the oxidation state of cobalt and the oxygen content.

Coulometric titration is used to examine the dependence of the oxygen deficiency of $Pr_{1-x}Sr_xCoO_{3-\delta}$ as a function of $p(O_2)$ at 973 K [25]. The oxygen non-stoichiometry of $Pr_{1-x}Sr_xCoO_{3-\delta}$ in Fig. 6 is obtained as a function of $p(O_2)$ at 973 K by coulometric titration in order to characterize the redox properties. The initial oxygen content of all samples is determined as 3.0 by TGA in air at room temperature, as shown in Fig. 6. The isotherms of $Pr_{1-x}Sr_xCoO_{3-\delta}$ have similar shapes, implying that they have nearly equivalent reduction mechanisms. All samples begin to decay at 10^{-4} atm and decomposition occurs at around 10^{-5} atm. The sample of $x = 0.5$ starts to show reduction at lower $p(O_2)$ than the other samples, and it is concluded that $Pr_{0.5}Sr_{0.5}CoO_{3-\delta}$ shows the best redox stability among $Pr_{1-x}Sr_xCoO_{3-\delta}$ series. Therefore, redox isotherm data in this study, $Pr_{1-x}Sr_xCoO_{3-\delta}$ operating at 10^{-5} atm at 973 K

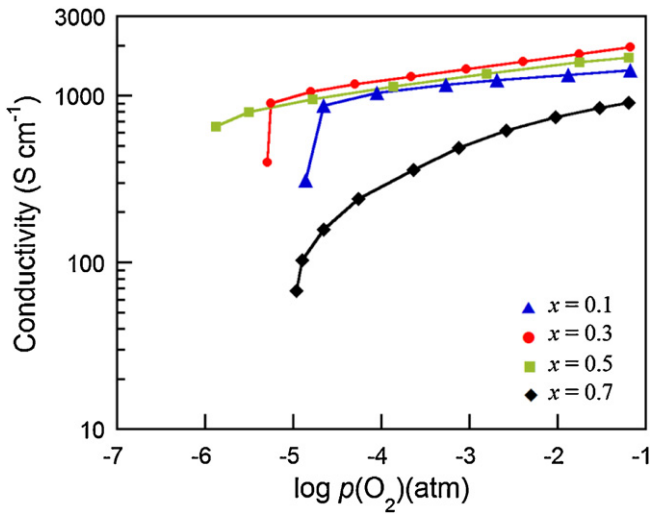

Fig. 7. Electrical conductivities of $Pr_{1-x}Sr_xCoO_{3-\delta}$ ($x = 0.1, 0.3, 0.5$, and 0.7) under various $p(O_2)$ (atm) at 973 K.

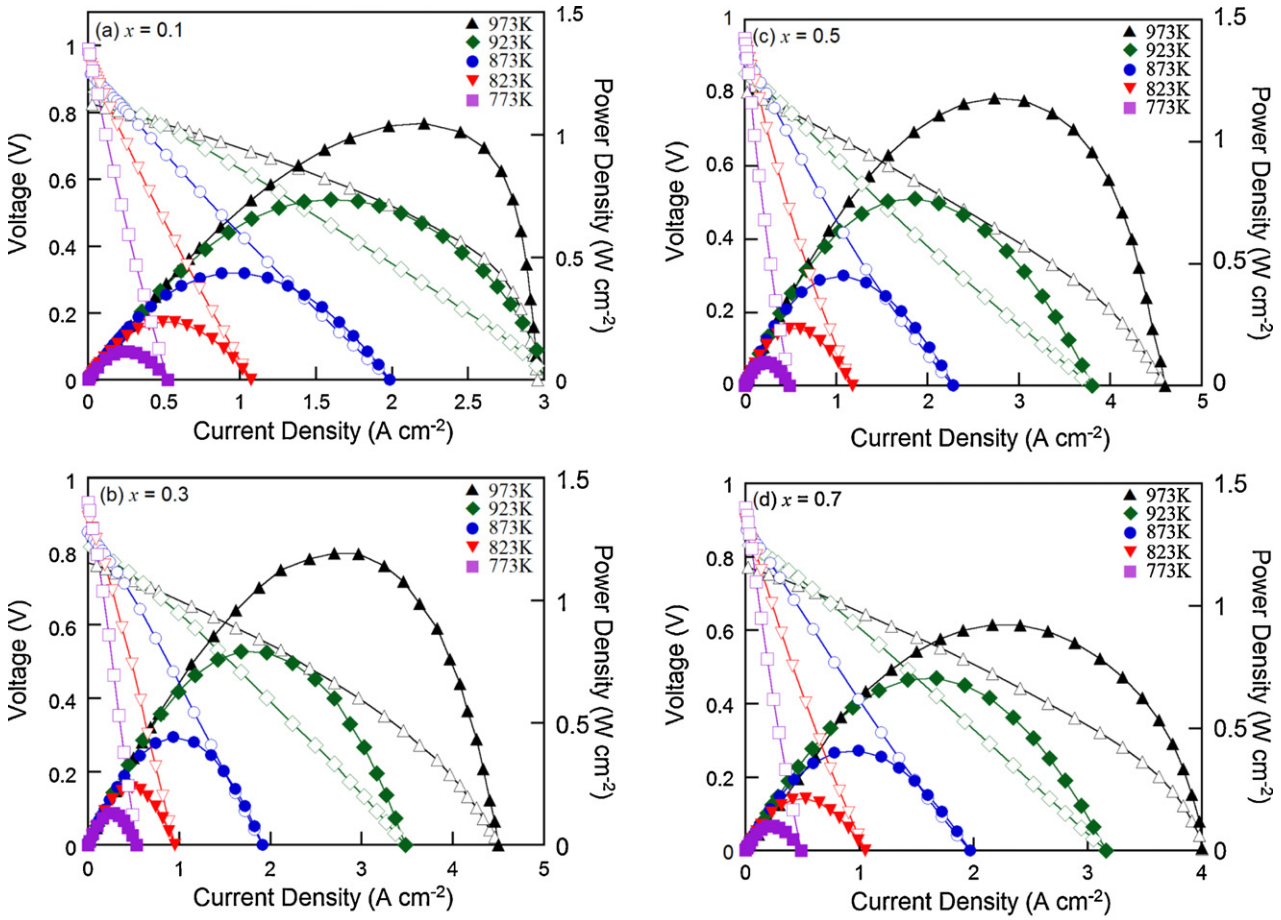

Fig. 8. *I–V* curves and corresponding power density curves of a single cell ($Pr_{1-x}Sr_xCoO_{3-\delta}$–GDC/GDC/Ni-GDC) under various temperatures: (a) $x = 0.1$, (b) $x = 0.3$, (c) $x = 0.5$, and (d) $x = 0.7$.

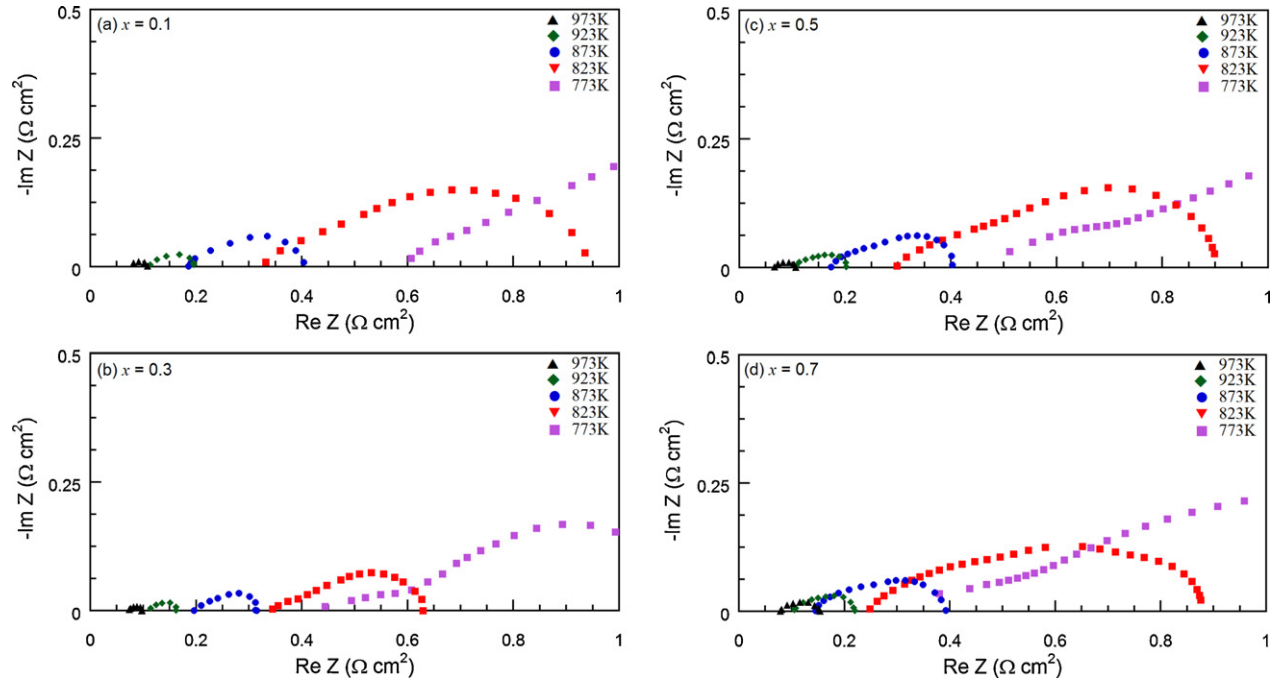

Fig. 9. Impedance spectra of a single cell ($Pr_{1-x}Sr_xCoO_{3-\delta}$–GDC/GDC/Ni-GDC) measured under OCV using H_2 as a fuel and ambient air as an oxidant at various temperatures: (a) $x = 0.1$, (b) $x = 0.3$, (c) $x = 0.5$, and (d) $x = 0.7$.

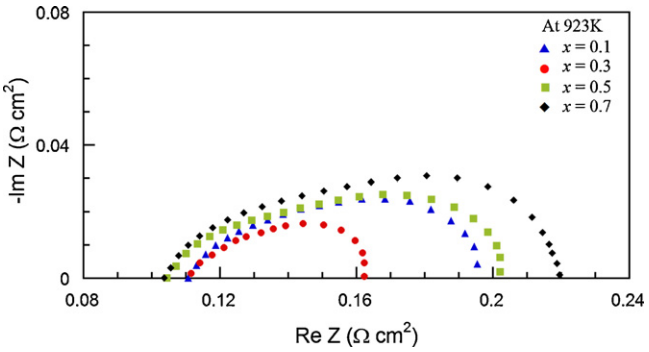

Fig. 10. Impedance spectra of the single cell ($Pr_{1-x}Sr_xCoO_{3-\delta}$–GDC/GDC/Ni-GDC) measured under OCV using H_2 as fuel and ambient air as oxidant at 923 K.

might undergo steep oxygen non-stoichiometry gradients and corresponding structural instability.

The 4-probe electrical conductivities of $Pr_{1-x}Sr_xCoO_{3-\delta}$ depending on the $p(O_2)$ at 973 K are presented in Fig. 7. The electrical conductivities increase with $p(O_2)$ in all cases, indicating that this material is a *p*-type electronic conductor under the present experimental conditions. The conductivities range from about 900 to 2000 S cm^{-1} at 973 K, which is sufficiently high for the IT-SOFC operating temperature. However, the electrical conductivities of $Pr_{1-x}Sr_xCoO_{3-\delta}$ significantly decrease at a $p(O_2)$ of approximately 10^{-6}–10^{-5} atm at 973 K. This suggests that the electrical properties are closely related with the decomposition of the material, which can be speculated from the oxygen nonstoichiometry in the isotherm data.

The electrochemical performances of the $Pr_{1-x}Sr_xCoO_{3-\delta}$ using a Ni-GDC anode supported cells are presented in Fig. 8 with humidified H_2 (3% H_2O) as a fuel and static ambient air as an oxidant in a temperature range of 773–973 K. The OCV for all samples is approximately 0.8 V at 973 K and increases with decreasing temperature. Generally, high oxygen vacancy concentration in a perovsikte type leads to an increase in the kinetics of oxygen exchange and diffusion of oxide ions in cathode materials, which in turn results in increased electrochemical performance [18]. The electrochemical performance trend of $Pr_{1-x}Sr_xCoO_{3-\delta}$, however, follows that of the electrical conductivity instead of the concentration of oxygen vacancy. Therefore, the effect of electronic charge compensation might overwhelm the oxygen ionic compensation. The maximum power density is 1.19 W cm^{-2} for $x = 0.3$ at 973 K. The other samples also show excellent power density, 1.16, 1.05, 0.92 W cm^{-2} for $x = 0.5$, 0.1, and 0.7, respectively.

The impedance spectra show similar trends with the power density, as seen in Fig. 9. For easier approach to recognize the impedance data at 923 K, Fig. 10 is additionally presented. In these spectra, the intercepts with the real axis at low frequency indicate the total resistance of the cell, and the value at high frequency is the ohmic resistance of the cell. The variation between the two values on the real axis indicates the sum of electrode–electrolyte interface resistance and electrode reactions, which is identified as the non-ohmic resistance of the cell [26]. The increase in operating temperature results in a considerable reduction of the non-ohmic resistance due to the faster oxygen reduction kinetics. The minimum non-ohmic resistance is 0.023 Ω cm^2 at 973 K for $x = 0.3$, *i.e.*, $Pr_{0.7}Sr_{0.3}CoO_{3-\delta}$.

4. Conclusions

$Pr_{1-x}Sr_xCoO_{3-\delta}$ ($x = 0.1$, 0.3, 0.5, and 0.7) perovskite oxides have been studied as a cathode material for IT-SOFCs. The $Pr_{1-x}Sr_xCoO_{3-\delta}$ powders are prepared by the Pechini method and the glycine-nitrate-process (GNP) method. The electrical conductivity of $Pr_{1-x}Sr_xCoO_{3-\delta}$ measured by a four-terminal DC arrangement increases with increasing Sr content but decreases at a high Sr doping range ($x > 0.3$) in air. For the samples with $x = 0.1$ and 0.3, Co^{4+} ions, which indicate the formation of electronic holes, maintain the electro-neutrality dominantly with strontium addition and result in higher electrical conductivity. On the other hand, the decreased electrical conductivity with higher Sr content for $x > 0.3$ is mostly caused by the formation of oxygen vacancies and a consequently decreased amount of Co^{4+} ions. The redox properties of $Pr_{1-x}Sr_xCoO_{3-\delta}$ are evaluated by coulometric titration, and electrical conductivity depending on $p(O_2)$ is measured simultaneously. All samples show similar isotherm shapes and start to decompose at around 10^{-5} atm at 973 K. The sample of $x = 0.5$ shows reduction at lower $p(O_2)$ than the other samples (at approximately 10^{-6} atm). The electrical performances of $Pr_{1-x}Sr_xCoO_{3-\delta}$ are evaluated using an anode-supported cell based on a GDC electrolyte with humidified H_2 (3% H_2O). The maximum power density is 1.19 W cm^{-2} for $x = 0.3$ at 973 K. The other samples also show good performance above 1.0 W cm^{-2}, except for $x = 0.7$. These results are explained by the higher electrical conductivity of the $Pr_{0.7}Sr_{0.3}CoO_{3-\delta}$, possibly due to the higher concentration of holes caused by electronic compensation rather than ionic compensation. Therefore, $Pr_{0.7}Sr_{0.3}CoO_{3-\delta}$ is a more suitable candidate cathode material for IT-SOFCs in terms of electrical conductivity and electrochemical performance.

Acknowledgements

This research was supported by the WCU (World Class University) program (R31-2009-000-20012-0), Mid-career Researcher Program (2011-0010773) through the National Research Foundation of Korea, funded by the Ministry of Education, Science and Technology, and the New & Renewable Energy of the Korea Institute of Energy Technology Evaluation and Planning (KETEP) grant (20113020030060) funded by the Korea government Ministry of Knowledge Economy.

References

[1] Z.P. Shao, S.M. Haile, J. Ahn, P.D. Ronney, Z.L. Zhan, S.A. Barnett, Nature 435 (2005) 795–798.
[2] A.J. Jacobson, Chem. Mater. 22 (2010) 660–674.
[3] B.C.H. Steele, A. Heinzel, Nature 414 (2001) 345–352.
[4] S.D. Park, J.M. Vohs, R.J. Gorte, Nature 404 (2000) 265–267.
[5] S.H. Choi, J.Y. Shin, G. Kim, J. Power Sources 201 (2012) 10–17.
[6] W. Zhou, R. Ran, Z. Shao, J. Power Sources 192 (2009) 231–246.
[7] J. Peña-Martínez, D. Marrero-López, D. Pérez-Coll, J.C. Ruiz-Morales, P. Núñez, Electrochim. Acta 52 (2007) 2950–2958.
[8] J. Wan, J.B. Goodenough, J.H. Zhu, Solid State Ionics 178 (2007) 281–286.
[9] Z. Shao, S.M. Haile, Nature 431 (2004) 170–173.
[10] J.M. Ralph, C. Rossignol, R. Kumar, J. Electrochem. Soc. 150 (2003) A1518–A1522.
[11] K.T. Lee, A. Manthiram, J. Electrochem. Soc. 152 (1) (2005) A197–A204.
[12] S.H. Choi, S. Yoo, J.Y. Shin, G. Kim, J. Electrochem. Soc. 158 (8) (2011) B995–B999.
[13] Y. Guo, H. Shi, R. Ran, Z. Shao, Int. J. Hydrogen Energy 34 (2009) 9496–9504.
[14] S.W. Baek, J. Bae, Y.S. Yoo, J. Power Sources 193 (2009) 431–440.
[15] M. Koyama, C.J. Wen, T. Masuyama, J. Otomo, H. Fukunaga, K. Yamada, K. Eguchi, H. Takahashi, J. Electrochem. Soc. 148 (2001) A795–A801.
[16] Y.L. Yang, C.L. Chen, S.Y. Chen, C.W. Chu, A.J. Jacobson, J. Electrochem. Soc. 147 (2000) 4001–4007.
[17] S.B. Adler, J.A. Lane, B.C.H. Steele, J. Electrochem. Soc. 143 (1996) 3554–3564.
[18] K.T. Lee, A. Manthiram, J. Electrochem. Soc. 153 (4) (2006) A794–A798.
[19] L. Dieterle, D. Bach, R. Schneider, H. Störmer, D. Gerthsen, U. Guntow, E. Ivers-Tiffée, A. Weber, C. Peters, H. Yokokawa, J. Mater. Sci. 43 (2008) 3135–3143.
[20] S. Yoo, J.Y. Shin, G. Kim, J. Mater. Chem. 21 (2011) 439–443.
[21] G.C. Kostogloudis, N. Vasilakos, C. Ftikos, Solid State Ionics 106 (1998) 207–218.
[22] M. Andersson, J. Yuan, B. Sunden, J. Appl. Energy 87 (2010) 1461–1476.
[23] J.H. Nam, D.H. Jeon, Electrochim. Acta 51 (2006) 3446–3460.
[24] A.N. Petrov, O.F. Kononchuk, A.V. Andreev, V.A. Cherepanov, P. Kofstad, Solid State Ionics 80 (1995) 189–199.
[25] S. Sengodan, J.H. Kim, J.Y. Shin, G. Kim, J. Electrochem. Soc. 158 (11) (2011) B1373–B1379.
[26] S. Adler, J.A. Lane, B.C.H. Steele, J. Electrochem. Soc. 143 (1996) 3554–3564.